JOURNAL OF MATERIALS SCIENCE 31 (1996) 4573–4580

Thermodynamical approach to the brittle fracture of dry plasters

P. COQUARD, R. BOISTELLE
Centre de Recherche sur les Mécanismes de la Croissance Cristalline, CNRS, Campus de Luminy, case 913, F-13288 Marseille cedex 09, France

The evolution of the fracture toughness, K_{Ic}, and fracture energy, G_{Ic}, of set plasters was determined on notched beams as a function of sample porosity, P, and characteristic size, W. Toughness was found to decrease with decreasing crack width. For set plasters of 57.7% porosity, the lowest toughness measured was $K_{Ic} = 0.13\ \text{MPa m}^{1/2}$ for a crack width of 0.2 mm. For this crack width, fracture toughness and fracture energy linearly changed with porosity: $K_{Ic} = 0.5\ (1–1.3\,P)\ \text{MPa m}^{1/2}$ and $G_{Ic} = 13.47\ (1–1.12\,P)\ \text{J m}^{-2}$. Dense plasters were more difficult to break than porous ones. The fracture energies were affected by the velocity of the fracture propagation, which induces damaging and multicracking of the material, so that the roughly calculated chemical surface energy of set plaster was too high. After correction it was estimated to be $0.4\ \text{J m}^{-2}$. Finally, because toughness increased with increasing sample size, it was concluded that fracture toughness and energy were not intrinsic parameters of the material. On the other hand, for our sample porosities and sizes, the reduced rupture force, $F_{rupt} W^{-0.65}$ is a constant and seems to be a characteristic parameter of the mechanical resistance of set plaster beams.

1. Introduction

Plaster is a much appreciated building material especially because it exhibits weak apparent densities and is a good phonic and thermic insulator, all these qualities arising from its high porosity. In addition, this highly porous material has a surprisingly high mechanical strength especially when it is dry. Several attempts have been made to quantify the mechanical properties of plaster as a function of its porosity [1–5]. It was shown that dry plaster is a linear elastic brittle material, but also that hardness, modulus of elasticity and strength do not properly describe the brittle fracture, especially in relation to strength, which is somewhat affected by the size of the samples [5]. This is also valid for some other brittle materials [6]. In order to describe the brittle fracture of plaster better, we used the linear elastic fracture mechanics (LEFM) theory.

Special attention was paid to the experimental conditions of the tests carried out on notched beams. Results are given in terms of fracture toughness and fracture energy which lead to microscopic considerations about the brittle fracture.

Finally, a study of fracture toughness was made as a function of sample size to decide whether fracture toughness is an intrinsic parameter of the brittle rupture of dry plaster. A new parameter is proposed to provide a better description of the brittle fracture of dry plaster.

2. Theory

The fracture mechanics concepts imply two conditions for achieving the fracture of a material. First, according to the energy balance proposed in Griffith's model [7], fracture occurs when the energy released by the crack propagation is large enough to supply the energy necessary to create new fractured surfaces. If G_c is the fracture energy and γ_{sg} the surface energy in Griffith's terminology, then fracture occurs when

$$G_c \geq 2\gamma_{sg} \tag{1}$$

If $G_c = 2\gamma_{sg}$, the rupture is controlled and the crack growth is slow. If $G_c \gg 2\gamma_{sg}$ the crack grows very rapidly and fracture is catastrophic. G_c is the critical strain energy release rate and gives an idea of the energy magnitude needed to extend the fracture and to produce a flat surface of unit area. This approach does not take into account the microscopic phenomena happening around the crack tip.

Second, for a homogeneous infinite linear elastic material, it was shown by Irwin [8] that the stress field around a crack can be characterized by a parameter K called the stress intensity. In the vicinity of the crack tip, the components of the stress tensor, σ_{ij}, take the form

$$\sigma_{ij} = \frac{K}{(2\Pi r)^{1/2}} f_{ij}(\theta) \tag{2}$$

0022–2461

where r and θ are the polar coordinates of the point where the stress tensor is calculated, f_{ij} is a function depending on the geometry of the sample and the way the stress is applied. K is therefore a stress-field parameter which links the magnitude of the stress intensity near the crack tip to both the stress applied to the solid structure and the geometry of the sample. K is independent of the material, but, when fracture occurs, it takes a critical value K_c, termed the fracture toughness. K_c is a property of the material and depicts its resistance to cracking.

In summary, fracture mechanics provides two parameters, G_c and K_c, which are supposed to describe intrinsically the material rupture and should be independent of the geometry of the sample. We shall come back to this subject later.

A crack can be stressed in three modes: I (cleavage), II (plane shear) and III (anti-plane shear). According to Kendall [9], only mode I is important when the sample undergoes flexion. When the crack propagates, the fracture toughness can be described by

$$K_{Ic} = Y\sigma_{rupt}a^{1/2} \tag{3}$$

where K_{Ic} is the critical stress intensity factor of mode I, σ_{rupt} the strength of the material, a the depth (length) of the fracture, and Y a parameter depending on the sample geometry. According to Paris and Sih [10], Y is a polynomial in a/W, where W is a characteristic dimension (Fig. 1) of the sample. For a single-edge notched sample loaded in a three-point flexural test with $L = 4W$, Y may be written, if $0.1 \leq a/W \leq 0.55$ [11]

$$Y = 1.93 - 3.07\frac{a}{W} + 14\left(\frac{a}{W}\right)^2 - 25.11\left(\frac{a}{W}\right)^3 + 25.8\left(\frac{a}{W}\right)^4 \tag{4}$$

Before determining K_{Ic} values, we can make the following comments. Equation 2 diverges when r tends to zero, i.e. in the vicinity of the crack tip, which means that the theory of elasticity does not really describe the behaviour of the material near the tip. According to Irwin, one way to deal with this discrepancy is to consider that the material exhibits some plasticity or is somewhat damaged around the crack tip, so that the theory of elasticity is no longer valid within a zone of radius R around the crack tip. R can be estimated [12] from

$$R \approx \frac{1}{\Pi}\left(\frac{K_{Ic}}{\sigma_{rupt}}\right)^2 \tag{5}$$

where σ_{rupt} is the strength of the material under consideration. In order that the LEFM theory is applicable, the damaged zone must be much smaller than the sample size and the following conditions must be fulfilled

$$a, b \geq 2.5\left(\frac{K_{Ic}}{\sigma_{rupt}}\right)^2 \tag{6a}$$

and

$$W \geq 5\left(\frac{K_{Ic}}{\sigma_{rupt}}\right)^2 \tag{6b}$$

Another possibility to check the size conditions is to consult Carpinteri's chart [13] where it is shown that in the case of a three-point flexural test, the LEFM theory is valid only if

$$S = \frac{K_{Ic}}{\sigma_{rupt}W^{1/2}} \leq 0.5 \tag{7}$$

If $S \geq 0.5$, the beam is damaged and the theory cannot explain the results. For each test, the value of S is given to check the accuracy of the experiment.

Taking into account Griffith's energy balance condition, and assuming that the material has a linear elastic behaviour, Irwin demonstrated [14] that fracture toughness can be related to Griffith's fracture energy, so that

$$G_{Ic} = \frac{K_{Ic}^2}{E} \tag{8}$$

where E is the modulus of elasticity of the material. Accordingly, Griffith's surface energy (Equation 1) is

$$\gamma_{sg} = \frac{G_{Ic}}{2} \tag{9}$$

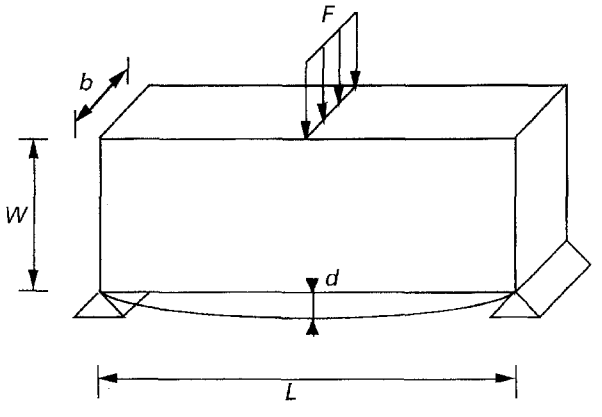

Figure 1 Characteristic dimensions of the notched beams used in the three-point bending test for measuring the fracture toughness.

3. Experimental procedure

Preparation of the plaster samples ($5 \times 25 \times 25$ cm^3) was described elsewhere [4, 5]. In short, set plaster, made of gypsum needles $CaSO_4 \cdot 2H_2O$, was obtained by hydration of α or β hemihydrate $CaSO_4$, $0.5\ H_2O$. Once the plaster had set, the needles formed a solid structure, the porosity of which ranged from 41–65 vol % as the water/hemihydrate ratio ranged from 50–109 wt %. The samples were dried at 42 °C and 20% relative humidity under atmospheric pressure because these conditions induce the best mechanical strength despite the fact that gypsum should slowly convert into hemihydrate, as shown by the thermodynamic phase diagram [4]. Fig. 2 is a typical scanning electron micrograph of a plaster with 65 vol % porosity.

The plaster beams used in the three-point flexion test where shaped by sawing the large samples prepared in the way previously described. To avoid

Figure 2 Typical aspect of a set plaster (65 vol % porosity) observed by scanning electron microscopy.

artefacts due to crystal orientation effects, all parts of the samples in contact with the walls of the moulds, were eliminated. In order to determine the evolution of fracture toughness and energy as a function of porosity, the beam dimensions (Fig. 1) were $L \times b \times W = 12 \times 1.5 \times 3\ cm^3$.

In the second part of our study, to detect a possible size effect of the sample on plaster toughness, the beam dimensions were chosen so that $L = 4W$, $b = 1.5$ cm and $a/W = 2$ with $W = 1$, 1.5, 3 and 5 cm and $b = 1.5$ cm.

It is noteworthy that the two beam types were homothetic with respect to their height W, distance L between the knife edges of the press and depth a of the crack.

Finally, to determine the different properties of the samples, we used a Hadamel-Lhormargy D Y 30 press, with an imposed strain rate of 0.1 mm min^{-1}.

4. Results

4.1. Influence of crack width

As the dimensions of the plaster beams were fixed, it was first necessary to check whether the crack dimensions (width and depth) had an influence on the fracture toughness. As the radius of curvature is difficult to appreciate, attempts were made to measure the fracture toughness as a function of the crack width, hoping to reach a lower limit which should be the intrinsic value of the fracture toughness. The cracks were shaped with saws the width of which ranged from 2–0.2 mm. In the latter case, the width was sometimes reduced by compression of the crack tip with a razor blade. The fracture toughness was measured on plaster samples exhibiting a porosity of 57.7%. The results are given in Table I. It is seen that toughness decreases with decreasing crack width but it is not certain if $K_{Ic} = 0.13$ MPa $m^{1/2}$ is the smallest possible value of K_{Ic} because cracks thinner than 0.2 mm could not be produced. It must be pointed out that the thinnest crack obtained with the razor blade indeed gave rise to the smallest K_{Ic} value, but not with the lowest standard deviation. For this reason, it was preferred to work with crack tips of 0.2 mm width which provided the lowest standard deviation of fracture toughness, bearing in mind that the measured K_{Ic} is not exactly the intrinsic parameter of plaster.

4.2. Influence of crack depth

The plaster beams used to measure the fracture toughness again had dimensions $L \times b \times W = 12 \times 1.5 \times 0.5$ cm^3 but the crack depths were adjusted so that $a/W = 0.2$, 0.4 and 0.5. Table II lists, for different crack depths, the fracture toughness, K_{Ic}, brittleness number, S, Young's modulus, E, rupture energy, G_{Ic}, and Griffith's surface energy, γ_{sg}, of plasters in the 41.4–65.0 vol % porosity range. Each fracture toughness was obtained from measurements carried out on at least eight samples. The standard deviation of the values is about 5% or less. The elasticity moduli were calculated from a model linking them to porosity [5]. The standard deviation of Young's moduli is about 10%. From this, the standard deviation of rupture energy was expected to be about 20%. From Table II, and from the previous considerations, it can be concluded that fracture toughness does not depend on the initial crack depth, at least in the depth range investigated here.

In the porosity range investigated, both fracture toughness (Fig. 3) and fracture energy (Fig. 4) can be described using a linear relationship with plaster

TABLE I Plaster toughness, K_{Ic}, and brittleness number, S, for different crack widths and depths (1*: +1 mm with a razor blade)

Crack shape	Width (mm)	Depth (mm)	K_{Ic} (MPa $m^{1/2}$)	S	Number of samples
	2	15	0.167 ± 8%	0.25	10
	1	15	0.149 ± 10%	0.23	14
	0.4	15	0.145 ± 5.6%	0.22	14
	0.4 + 0.2	13 + 2	0.139 ± 5%	0.21	14
	0.4 + 0.2	12 + 2 + 1*	0.130 ± 7.5%	0.20	10

TABLE II Evolution of plaster toughness, K_{Ic}, for three crack widths (mm), brittleness number, S, Young's modulus, E, rupture energy, G_{Ic}, and Griffith surface energy, γ_{sg}, as a function of water/hemihydrate ratio and corresponding porosity, P

	Water/hemihydrate ratio									
	0.5	0.65	0.68	0.74	0.775	0.80	0.82	0.93	1.05	1.09
P (vol%)	0.414	0.51	0.525	0.55	0.56	0.57	0.577	0.6	0.638	0.65
K_{Ic} 0.5 mm	0.245	0.161	0.156	0.151	0.147	0.142	0.13	0.111	0.096	0.086
0.4 mm	–	0.167	–	–	0.14	0.134	–	0.117	0.094	–
0.2 mm	–	0.175	–	–	0.152	0.139	–	0.116	0.055	–
$\bar{K}_{Ic}$	0.245	0.167	0.156	0.151	0.146	0.139	0.13	0.114	0.095	0.086
S	0.19	0.23	0.18	–	0.23	–	0.19	0.23	0.23	0.17
E^* (GPa)	8.14	5.26	4.86	4.23	3.99	3.76	3.6	3.09	2.34	2.12
G_{Ic} (J m^{-2})	7.37	5.3	5	5.39	5.34	5.13	4.69	4.2	3.85	3.48
γ_{sg} (J m^{-2})	3.68	2.6	2.5	2.69	2.67	2.565	2.345	2.1	1.92	1.74
γ_{sg} (J m^{-2}) $P = 0$	6.28	5.3	5.26	5.97	6.06	5.96	5.54	5.25	5.3	4.97

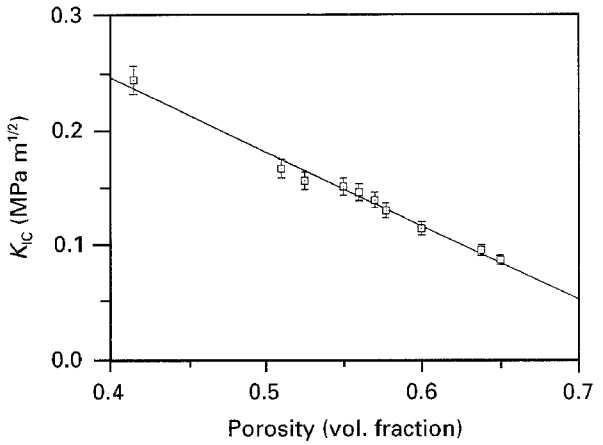

Figure 3 Fracture toughness of dry set plasters as a function of their porosity.

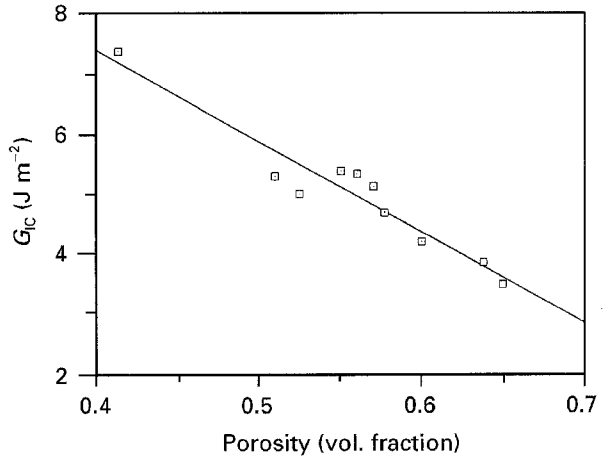

Figure 4 Fracture energy of dry set plasters as a function of their porosity.

porosity

$$K_{Ic} = 0.5(1\text{–}1.3\ P)\ \text{MPa m}^{1/2} \qquad (r^2 = 0.986) \quad (10a)$$

$$G_{Ic} = 13.47(1\text{–}1.12\ P)\ \text{J m}^{-2} \qquad (r^2 = 0.921) \quad (10b)$$

Accordingly, dense plasters are more difficult to break than more porous ones. In addition, γ_{sg} varies like G_{Ic}, so that

$$\gamma_{sg} = \gamma_{sg(0)}(1 - P) \qquad (11)$$

where $\gamma_{sg(0)}$ is Griffith's surface energy at porosity $P = 0$.

It turns out that $\gamma_{sg(0)}$ is about 6–7 J m^{-2}, a value which is much larger than those usually determined by cleavage of single crystals [15]. Accordingly, it may be possible to find the physical significance of Griffith's surface energy by means of mechanical tests.

4.3. Analysis of the fracture energy

Figs 5 and 6 show the typical aspect of a notched sample after crack propagation. At low magnification (Fig. 5) we first note that the main fracture is very rough so that the area of the crack is much larger than the area deduced from the geometrical section. At higher magnification (Fig. 6) we also see that around the main crack there is an important network of side cracks. These secondary cracks do not directly contribute to the breakdown of the solid but they obviously consume part of the rupture energy. For estimating the amount of energy really spent to open the main crack, it is necessary, as far as possible, to estimate the real fracture area issued from the propagation of the main crack in the sample. In order to estimate this crack area, attempts were made to estimate its real length by measuring, step-by-step on a photograph, crack pieces of about 10 μm. It was found that the crack was at least 1.6 times longer than the value previously obtained assuming that the crack is a straight line. If this is valid for the direction normal to the crack propagation, the real value of G_{Ic} would be at least $(1.6)^2$ smaller than that previously calculated.

Taking account of the surface correction, for a plaster of porosity $P = 57.7\%$, the fracture energy of which is about 5 J m^{-2}, leads to $\gamma_{sg} \approx 1$ J m^{-2}. These values become more comparable to those obtained by cleaving single crystals of minerals [15].

Now, to distinguish the energy really spent to open the main crack, from that spent in damaging and multi-cracking the material, we can recall some results obtained by studying the slow propagation of cracks through different materials. Such studies carried out on glasses [16] and polycrystalline ceramics [17] showed that it is possible to detect crack propagation prior to material rupture. For dry set plasters [18],

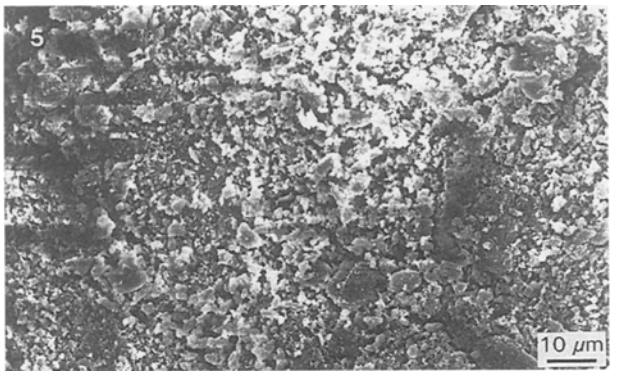

Figure 5 Lateral view of a cracked notched beam.

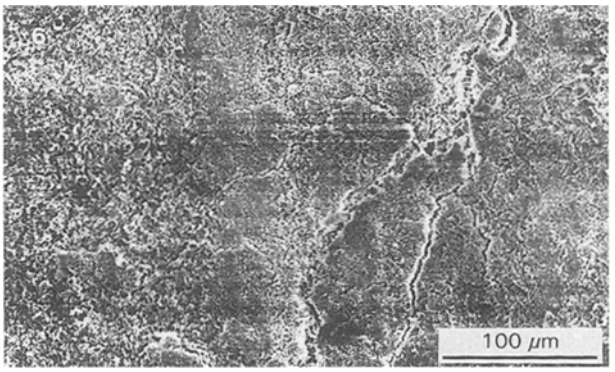

Figure 6 Lateral network of side cracks originating from a main crack developed at a high propagation rate.

catastrophic failure of the samples occurs when the crack velocity, V, exceeds $1 \times 10^{-4}\,\mathrm{m\,s^{-1}}$. Fig. 7 shows Williams and Marshall's results [17] for an inorganic glass and those of Takatsu *et al.* [18] for a dry plaster of 53.3% porosity. In the former case, the sample was placed in dry paraffin or in water. In paraffin, the results depended on the stress intensity applied to the sample. When the stress, K_I, was small, the crack propagation was slow: it was the chemical reaction (adsorption, diffusion) near the crack tip which controlled the propagation rate. At intermediate stress intensities, diffusion of corrosive species towards the crack was rate controlling. At high stress intensities, a mixture of corrosive and mechanical failure takes place. According to Maugis [19], the sole case where the crack propagation energy is twice Griffith's surface energy, is the case where the crack propagation is very slow, about $1 \times 10^{-10}\,\mathrm{m\,s^{-1}}$ for brittle solids. Only in that case does G_I correspond to the chemical energy spent to open the main crack, because, for very low crack propagation rates, there is no multi-cracking around the main crack.

For plasters, the crack energy is not known for such low crack velocities, as the slowest rate measured on plasters is about $1 \times 10^{-7}\,\mathrm{m\,s^{-1}}$ [18]. Accordingly, (Fig. 7), it is likely that under such conditions the crack energy mainly corresponds to a mechanical failure and has nothing to do with a pure chemical surface energy. However, if we assume a linear relationship between $\ln K_I$ and $\ln V$ (Fig. 7), a linear regression on Takatsu *et al.*'s results [18] yields

$$\ln K_I = 0.029 \ln V - 1.57 \qquad (12)$$

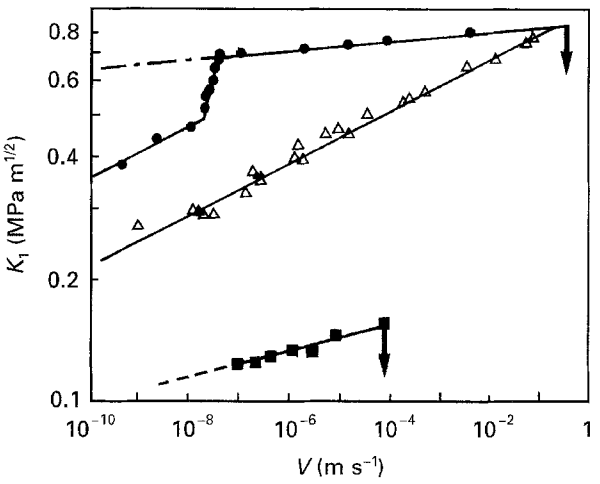

Figure 7 Growth rate of cracks propagating in an inorganic glass immersed in (△) water or (●) paraffin [17] and (■) in a plaster of 53 vol % porosity immersed in paraffin [18].

so that for a dry plaster with 53.3% porosity

$$K_I = K_{Ic} = 0.16\,\mathrm{MPa\,m^{1/2}} \qquad \text{for } V = 1 \times 10^{-4}\,\mathrm{m\,s^{-1}} \qquad (13a)$$

$$K_I = 0.106\,\mathrm{MPa\,m^{1/2}} \qquad \text{for } V = 1 \times 10^{-10}\,\mathrm{m\,s^{-1}} \qquad (13b)$$

It is noteworthy that the fracture toughness determined by Takatsu *et al.* is consistent with our results. Taking a mean value [5] of 5.5 GPa for the modulus of elasticity of plaster, we have

$$G_I = G_{Ic} = 4.58\,\mathrm{J\,m^{-2}} \qquad \text{for } V = 1 \times 10^{-4}\,\mathrm{m\,s^{-1}} \qquad (14a)$$

$$G = 2\gamma_{sg} = 2.05\,\mathrm{J\,m^{-2}} \qquad \text{for } V = 1 \times 10^{-4}\,\mathrm{m\,s^{-1}}. \qquad (14b)$$

Taking the fracture roughness into account (1.6×1.6 correction term) the chemical surface energy of set plaster should be $\gamma_s \sim 0.4\,\mathrm{J\,m^{-2}}$.

Finally, because $\gamma_{sg} \sim 1\,\mathrm{J\,m^{-2}}$, it results that about $0.6\,\mathrm{J\,m^{-2}}$ is spent for damaging and multicracking the material. This value is of the same order of magnitude as those obtained by cleavage of single crystals of ionic crystals such as NaCl, LiF, $CaCO_3$ [15].

4.4. Sample size and fracture toughness

Tensile or flexion strengths of unnotched beams are dependent, for some brittle materials, on sample size [5, 6]. In addition, even for the same size, reproducibility of the results is rather poor. On notched beams, the standard deviation obtained in the values of fracture toughness was reduced to about 5% but up to now, no comment has been made on the eventual variation of fracture toughness with sample size. To investigate this parameter, samples were shaped as shown in Fig. 1, under the conditions that $L = 4W$, $W = 1, 1.5, 3$ and $5\,\mathrm{cm}$, $b = 1.5\,\mathrm{cm}$ and $a = W/2$. Such samples are homothetic in length, height and crack depth but not in thickness. Homothety could not be strictly kept for technical reasons: the largest samples would have been too large for our press,

TABLE III Plaster toughness, K_{Ic}, for different hydration ratios, Wa/He, and sample sizes, W.

Wa/He	Sample size, W (mm)											
	1			1.5			3			5		
	K_{Ic} (MPa m$^{1/2}$)	S.D.	No. of samples	K_{Ic} (MPa m$^{1/2}$)	S.D.	No. of samples	K_{Ic} (MPa m$^{1/2}$)	S.D.	No. of samples	K_{Ic} (MPa m$^{1/2}$)	S.D.	No. of samples
1.09	0.073	± 0.009	15	0.079	± 0.007	13	0.087	± 0.008	7	0.092	± 0.007	5
0.82	0.103	± 0.004	21	0.117	± 0.008	16	0.13	± 0.01	7	0.144	± 0.007	6
0.68	0.139	± 0.018	16	0.149	± 0.01	15	0.154	± 0.009	8	0.150	± 0.002	4
0.50	0.191	± 0.012	10	0.215	± 0.009	10	0.245	± 0.019	10	0.25	± 0.007	6

whereas the smallest samples would have given rise to rupture strengths less than 10 N and not measurable with good accuracy.

The results obtained with four sample sizes of the same geometry are given in Table III for plasters of different porosity and composition. Standard deviations and the number of samples tested are also given. Fracture toughness increases with increasing sample size. Accordingly we must conclude that fracture toughness and fracture energy are not intrinsic parameters of the material and that another formalism should be found to describe the mechanical resistance of plaster.

5. Discussion

The fact that the chemical surface energy of dry plaster is about 0.4 J m^{-2} suggests that the crystals in contact are linked by ionic bonds, notwithstanding that, on a macroscopic scale, they are completely disordered with respect to each other. Only ionic bonds are strong enough to explain the mechanical resistance of such a disordered structure. Even if nucleation and growth of each gypsum crystallite occur randomly prior to setting, it seems that some microscopic rearrangement of the interfaces accompanies hardening. The LEFM theory does not suppose any variation of the fracture toughness with sample size. For the three-point flexure test, the strength of the sample is calculated from the rupture force of the sample, and from its geometry L, b, W

$$\sigma_{rupt} = \frac{3}{2}\frac{F_{rupt}L}{bW^2} \tag{15}$$

where F_{rupt} is the rupture force of the sample. If this value of F_{rupt} is inserted in Equation 3, bearing in mind that $a/W = 2$, $L = 4W$ and b is constant, it turns out from Equations 3 and 4 that

$$K_{Ic} = F_{rupt}W^{-1/2}\text{Cte} \tag{16}$$

According to the LEFM theory, K_{Ic} should be constant. In this hypothesis, it turns out that

$$F_{rupt}W^{-1/2} = \text{Cte} \tag{17}$$

If Weibull's theory is applied [4, 20] to samples of sizes i and j having volume V_i and V_j and mean rupture strengths σ_i and σ_j, we can write for unnotched beams

$$\sigma_i V_i^{1/m_i} = \text{Cte} \tag{18}$$

with

$$\sigma_i = \frac{3}{2}\frac{F_{rupt_i}L_i}{bW_i^2} \tag{19}$$

and

$$V_i = bW_iL_i \tag{20}$$

m_i, being Weibull's moduli. In our case, with $L = 4W$ and $b = \text{Cte}$, Equation 17 can be rewritten as

$$F_{rupt}W^{2/m_i - 1} = \text{Cte} \tag{21}$$

For a mean Weibull's modulus $m = 9$ [5], we have

$$F_{rupt}W^{-0.78} = \text{Cte} \tag{22}$$

Because the theory of elasticity and the LEFM theory poorly describe the experimental data but lead to scaling laws linking rupture force and sample size, an attempt was made to analyse the results obtained on notched beams using this formalism. More precisely, the evolution of the rupture forces was studied as a function of the characteristic dimension, W, of the samples: for each plaster $\ln F_{rupt}$ was plotted against $\ln W$ (Fig. 8). By linear regression, for plasters of 65 vol % porosity, we found $F_{rupt}W^{\alpha} = \text{Cte}$ for $\alpha = -0.65 \pm 0.09$. Table IV shows the results obtained with plasters of different porosities. It turns out that $F_{rupt}W^{-0.65}$ may be considered as a reduced rupture force of plasters, independent of sample size.

In addition, the exponent $\alpha = -0.65 \pm 0.09$ seems to be independent of plaster porosity. The present reduced rupture force may, therefore, be considered as an intrinsic parameter of plaster at least for the sample geometry and sizes investigated here. As α is clearly different from -0.50, which would be the characteristic exponent of W in the LEFM theory, it can also be concluded that this theory cannot account for the evolution of the mechanical strength of plasters as a function of size.

It is also noteworthy that the reduced rupture strength can be used now to standardize the mechanical properties of plaster and predict the rupture force of any plaster of any size. Fig. 9 shows the evolution of the reduced rupture strength for plasters of different porosities from which it is easy to deduce the rupture stress, F_{rupt}, of the material knowing its characteristic

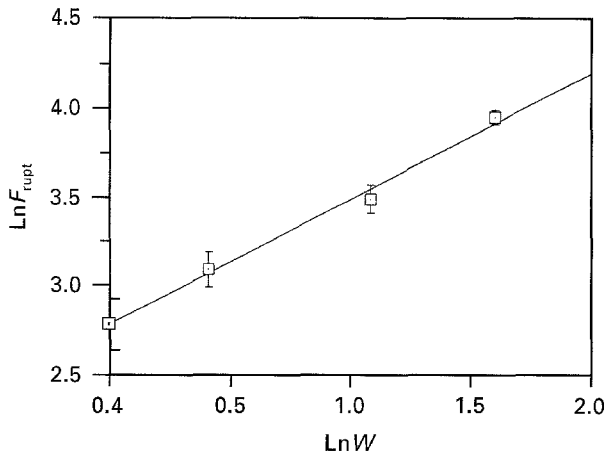

Figure 8 Scaling law between the mean rupture force and the characteristic size of plaster samples (porosity = 57.7%).

TABLE IV Exponents, α, of the reduced rupture force $F_{rupt}W^{-\alpha} = Cte$ for plasters produced with different water/hemihydrate ratios

Wa/He	$F_{rupt}W^{-\alpha} = Cte$	
	α	r^2
1.09	0.65 ± 0.11	0.998
0.82	0.67 ± 0.04	0.985
0.68	0.55 ± 0.06	0.993
0.50	0.64 ± 0.05	0.989

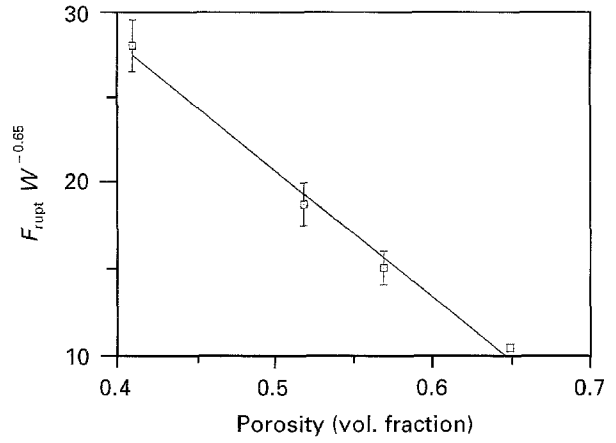

Figure 9 Reduced rupture strength for plasters of different porosities.

dimension, W. However, it must be pointed out that the validity of our model should be confirmed using much larger solid structures, because, for technical reasons, we could not investigate homothetic samples longer (L) than 20 cm and thicker (W) than 5 cm.

We can at least add that this new approach to brittle material mechanics, using a reduced rupture force, is supported by numeric simulations describing the brittle fracture of two-dimensional networks of beams. In these simulations, the constitutive beams of the lattice all have the same elasticity, but various breaking thresholds drawn at random from a continuous distribution [21, 22]. It appears that the reduced rupture force, $F_{rupt}W^{\alpha}$, is a characteristic parameter of the mechanical resistance of brittle materials, especially because it is not size dependent. This work is one of the first attempts to extend to real three-dimensional materials the theories which were proposed to rule the fracture of two-dimensional brittle structures.

6. Conclusion

From previous experiments, we conclude that the LEFM theory, which supposes that the solid exhibits a good homogeneity around the tip of the growing crack, does not properly describe the brittle fracture of set plasters. This theory involves the rupture stress being independent of sample size, which is not the case. Nevertheless, the data obtained from fracture experiments on notched beams can be used to define a new intrinsic parameter of the brittle fracture, free of assumptions concerning the material structure: the reduced rupture force, $F_{rupt}W^{-0.65}$, allows plasters to be classified as a function of their resistance. As the exponent of W seems to be independent of the plaster, it is possible to classify any new plaster as soon as rupture force and size are known. However, it is noteworthy that these conclusions are drawn from results obtained with a certain sample geometry and size. They should be verified on samples exhibiting smaller and larger sizes.

Considering that the LEFM theory gives comparative results at constant sample size, it was interesting to analyse the energetic content of the fracture energy. Taking account of the important roughness of the fractured surfaces, and of the velocity of the crack propagation, it could be deduced that the chemical surface energy of plaster was around 0.4 J m^{-2}, so that more than 50% of the energy spent to develop a crack is lost in damaging and multicracking the material. We conclude that the cohesion of plaster is due to electrostatic interactions between the microcrystals which form the solid structure.

References

1. V. M. RÖBLER and I. ODLER, *Zement Kalk Gyps Int.* **2** (1989).
2. I. SOROKA and P. J. SEREDA, *J. Am. Ceram. Soc.* **51** (1967) 6.
3. K. K. PHANI and S. K. NIYOGI, *J. Mater. Sci.* **22** (1987) 257.
4. P. COQUARD and R. BOISTELLE, *Int. J. Rock. Mech. Min. Sci.* **31** (1994) 517.
5. P. COQUARD, R. BOISTELLE, L. AMATHIEU and P. BARRIAC, *J. Mater. Sci.* **29** (1994) 4611.
6. A. CARPENTERI, Nota Technica 73, ISCB 1983, University of Bologna, Italy.
7. A. A. GRIFFITH, *Phil. Trans. R. Soc.* **A221** (1920) 163.
8. G. R. IRWIN, *Appl. Mater. Res.* **3** (1973) 65.
9. K. KENDALL, *Proc. R. Soc.* **A261** (1978) 245.
10. P. C. PARIS and G. C. SIH, ASTM STP **381** (American Society for Testing and Materials, Philadelphia PA, 1965) p. 30.
11. Norme française NF A 03-180 (1981) and Norme ASTM E 399-83.
12. F. BURESCH, "Fracture Mechanics of Ceramics", Vol. 4, (Plenum Press, New York, 1978) p. 835.
13. A. CARPENTERI, *Eng. Fract. Mech.* **16** (1982) 467.
14. G. R. IRWIN, *Appl. Mater. Res.* **3** (1964) 65.

15. J. J. GILMAN, *J. Appl. Phys.* **31** (1960) 2208.
16. A. G. EVANS, *J. Mater. Sci.* **7** (1972) 1137.
17. J. G. WILLIAMS and G. P. MARSHALL, *Proc. R. Soc.* **A342** (1975) 55.
18. M. TAKATSU, K. SHIMOMURA, I. TAKAHASHI and T. ONO, *Gypsum Lime* **173** (1981) 15.
19. D. MAUGIS, *J. Mater. Sci.* **20** (1985) 3041.
20. W. WEIBULL, *J. Appl. Mech.* **18** (1951) 293.
21. H. J. HERRMANN and S. ROUX, "Statistical Models for the Fracture of Disordered Media" (Amsterdam, 1990) Ch. 7.
22. L. DÉ ARCANGELIS, A. HANSEN, H. J. HERRMANN and S. ROUX, *Phys. Rev. B* **40** (1989) 877.

Received 4 April 1995
and accepted 13 February 1996